THE ASTRONOMICAL JOURNAL VOLUME 82, NUMBER 12 DECEMBER 1977

A numerical approach to the testing of the fission hypothesis

L. B. Lucy[a)]
Institute of Astronomy, Cambridge, United Kingdom
European Southern Observatory, Geneva, Switzerland
(Received 12 August 1977; revised 16 September 1977)

A finite-size particle scheme for the numerical solution of two- and three-dimensional gas dynamical problems of astronomical interest is described and tested. The scheme is then applied to the fission problem for optically thick protostars. Results are given, showing the evolution of one such protostar from an initial state as a single, rotating star to a final state as a triple system whose components contain 60% of the original mass. The decisiveness of this numerical test of the fission hypothesis and its relevance to observed binaries are briefly discussed.

INTRODUCTION

THE hypothesis that fission is the mechanism by which close binaries are formed has regained favor in recent years. Those responsible for this revival (Lynden-Bell 1964, 1965; James 1964; Stoeckly 1965; Roxburgh 1966; Bodenheimer and Ostriker 1970; Lebovitz 1972, 1974) have rebutted earlier theoretical objections (see also Ostriker 1970) and have discussed the hypothesis in the context of our current understanding of pre-main-sequence evolution. The early history of the fission hypothesis and the related investigations into the figures of equilibrium of rotating liquids has been summarized by Chandrasekhar (1969).

Although fission is now commonly considered to be the most likely explanation for the existence of close binaries, the hypothesis cannot be regarded as proved until the evolution of a rotating protostar has been followed from an initial state as a single star to a final state as a detached binary system. This is a formidable problem, however, since it requires the ability to compute the three-dimensional motion of a self-gravitating, compressible gas. Fortunately, some simplifying circumstances make it less than forbidding. First, the high frequency of close binaries over a wide mass range surely implies that no special characteristics of the properties of stellar matter are essential to binary formation; consequently, these properties need not be treated accurately.

A second and crucial simplification concerns the spatial resolution of the calculation. Because the initial departure from axial symmetry is due to the onset of dynamical overstability for a mode of low order, we might reasonably hope that the subsequent evolution can be adequately followed with a low-resolution description of the protostar's structure. If this is indeed so, the problem can be tackled with present-day computers.

On the assumption, therefore, that a decisive test of the fission hypothesis might be provided by a three-dimensional gas dynamical calculation of low spatial resolution, the bulk of this paper is devoted to describing (Sec. II) and testing (Sec. III) a numerical scheme for carrying out such calculations. This scheme is then used (Sec. IV) to follow the contraction of a rotating protostar and results illustrating the fission mechanism are obtained.

I. ASSUMPTIONS AND EQUATIONS

In this section, after stating our assumptions, we derive the basic equations in the form used when applying the numerical technique of Sec. II.

(*a*) *Assumptions.* A rotating, axisymmetric, optically thick protostar of homogeneous composition will be the starting point of the calculation, and this protostar's evolution will be followed up to and beyond the point of instability to a nonaxisymmetric perturbation. To ensure that contraction does not halt prior to this point, energy generation by nuclear burning will be omitted. Accordingly, the basic equations are those describing the motion of a self-gravitating, compressible gas with entropy changes occurring only as a result of radiative conduction.

In accordance with the argument that the detailed properties of stellar matter cannot be of decisive importance, we assume that the matter is a fully ionized perfect gas and that radiation pressure may be neglected; the ratio of specific heats γ and the mean molecular weight μ are then constants. In addition, we assume that the opacity κ is independent of state variables.

(*b*) *Units.* In the interest of computational accuracy, it is useful to express dimensions in terms of a time-dependent length scale $R(t)$ chosen so as to largely eliminate the protostar's contraction. We also adopt $\mathcal{M}$, the protostar's mass, as the unit of mass, $\tau_* = (R^3/G\mathcal{M})^{1/2}$ as the unit of time, and $T_* = (\mu m_H/k)(G\mathcal{M}/R)$ as the unit of temperature. In terms of these basic units, we now take R/τ_* to be the unit of velocity, $1/\tau_*$ to be

[a)] Permanent address: Department of Astronomy, Columbia University, New York, NY 10027.

the unit of angular velocity, $G\mathcal{M}/R$ to be the unit of potential, $\mathcal{M}/R^3$ to be the unit of density, $G\mathcal{M}^2/R^4$ to be the unit of pressure, and $F_* = (16/3)(R^2/\kappa\mathcal{M})(\sigma T_*^4)$ to be the unit of radiative flux.

(*c*) *Equations.* With all quantities expressed in terms of these *time-dependent* units, the rates of change of the position $\mathbf{r}$ and velocity $\mathbf{v}$ of an element of gas are given by the equations

$$\frac{d}{d\tau}(R^{-1/2}\mathbf{v}) = R^{-1/2}\left(-\frac{1}{\rho}\nabla P - \nabla\phi\right), \tag{1}$$

$$\frac{d}{d\tau}(R\mathbf{r}) = R\mathbf{v}, \tag{2}$$

where ϕ, the gravitational potential, satisfies Poisson's equation,

$$\nabla^2\phi = 4\pi\rho. \tag{3}$$

If we now define

$$S = (\gamma - 1)^{-1}\ln(P/\rho^\gamma) \tag{4}$$

as a specific entropy variable, its rate of change following an element of gas is given by the equation

$$T\left(\frac{dS}{d\tau} + \chi\frac{d\ln R}{d\tau}\right) = -\frac{\lambda}{\rho}\nabla\cdot\mathbf{F}, \tag{5}$$

where $\chi = (3\gamma - 4)/(\gamma - 1)$ and $4\pi\lambda = \tau_*/(G\mathcal{M}^2/RL_*)$ with $L_* = 4\pi R^2F_*$. For the radiative flux $\mathbf{F}$, we adopt the usual conductivity approximation,

$$\mathbf{F} = -\frac{T^3}{\rho}\nabla T, \tag{6}$$

since the protostar is assumed to be optically thick.

The system of equations is completed by the equation of state,

$$P = \rho T. \tag{7}$$

The equation of continuity is omitted since the adopted numerical scheme (Sec. II) conserves mass automatically.

As initial conditions, we must specify $\mathbf{v}$, S, and ρ as functions of position at $\tau = 0$. As boundary conditions, we require that

$$|\nabla\phi| \to |\mathbf{r}|^{-2} \quad \text{as } |\mathbf{r}| \to \infty \tag{8}$$

and that

$$T = 0 \quad \text{when } \rho = 0, \tag{9}$$

which is well known to be an acceptable surface boundary condition for stars with radiative envelopes.

(*d*) *Scale Factor.* We now specify the hitherto arbitrary scale factor $R(t)$ by taking it to be the radius of the homologously contracting spherical protostar that, apart from having no angular momentum, is identical with our rotating protostar. (That a solution with homologous contraction exists is a consequence of the simplicity of our assumptions about κ, μ, and γ.)

With this choice of scale factor, the structure of the homologously contracting star is stationary and of unit radius in the contracting coordinate system. The structure of this star may therefore be obtained from the above equations by finding the time-independent, spherically symmetric solution that satisfies the conditions: $\mathcal{M}_r = L_r = 0$ at $r = 0$, and $\rho = T = 0$ at $r = 1$. If inertial forces are neglected in the momentum equation, the ordinary differential equations governing the structure of this star reduce to the usual equations of stellar structure with energy generation rate

$$\epsilon_g = \nu T, \tag{10}$$

where ν is given by the equation

$$\frac{d\ln R}{d\tau} = -\frac{\nu\lambda}{\chi}. \tag{11}$$

Because the surface boundary conditions for this model are applied at a specified radius, a solution exists only for a particular value of ν, which is therefore an eigenvalue. Using a Henyey code, we find that

$$\nu = 0.256 \tag{12}$$

and the corresponding structure is such that $L = 0.119L_*$ and $\rho_c/\bar{\rho} = 38.8$.

With ν now known, Eq. (11) determines the e-folding time for the contraction of this model—and, therefore, also of the coordinate system used in following the structural changes of the rotating protostar. If this contraction time scale is compared to that of a polytrope of the same mass, radius, and luminosity, agreement is found for $n = 2.85$, which may therefore be regarded as the effective polytropic index of the spherical model.

II. NUMERICAL SCHEME

We now describe a numerical scheme for obtaining approximate solutions of the equations in Sec. I.

(*a*) *Monte Carlo Theory.* Let us first consider the problem of approximating the function,

$$\eta(\mathbf{r}) = \int_V w(\mathbf{r} - \mathbf{r}')\xi(\mathbf{r}')\rho(\mathbf{r}')dV', \tag{13}$$

where $\rho \geq 0$. According to standard Monte Carlo theory (see, e.g., Hammersley and Handscomb 1964), if a set of J points $\mathbf{r}_j$ are randomly distributed in V in such a way that the probability of a point being found in the volume element dV' at $\mathbf{r}'$ is proportional to $\rho(\mathbf{r}')dV'$, then

$$\tilde{\eta}(\mathbf{r}) = \frac{1}{J}\sum_j w(\mathbf{r} - \mathbf{r}_j)\xi(\mathbf{r}_j) \tag{14}$$

converges to $\eta(\mathbf{r})$ as $J \to \infty$.

If we now suppose that

$$\int_V w(\mathbf{r}-\mathbf{r}')dV' = 1 \tag{15}$$

and

$$w = 0 \quad \text{for } |\mathbf{r}-\mathbf{r}'| > \sigma, \tag{16}$$

then $\eta(\mathbf{r}) \to \xi(\mathbf{r})\rho(\mathbf{r})$ as $\sigma \to 0$. It therefore follows that

$$\tilde{\eta}(\mathbf{r}) \to \xi(\mathbf{r})\rho(\mathbf{r}) \quad \text{as } J \to \infty \text{ and } \sigma \to 0. \tag{17}$$

(*b*) *Basic Idea.* In this scheme, the evolution of the protostar is followed by computing the histories of a finite set of its constituent gas particles. At time τ, therefore, the state of the protostar will be represented by the positions $\mathbf{r}_j$, the velocities $\mathbf{v}_j$, and the specific entropies S_j of J *macroscopic* gas particles, and this discrete representation will be advanced to time $\tau + \Delta\tau$ using difference equations to approximate Eqs. (1), (2), and (5).

The difference equations for Eqs. (1) and (5) must provide a means of approximating the space derivatives in ∇P and $\nabla\cdot\mathbf{F}$, but how to do this is far from obvious since the positions $\mathbf{r}_j$ at which information is available do not define a cubical grid. In the adopted technique, this problem is solved by applying Monte Carlo theory to the *discrete* representation in order to obtain *continuous* representations of the spatial variations of two state variables; analytical differentiation then gives the required space derivatives.

If we stipulate that the *broadening function* w be a continuous function of position, then a continuous function approximating the mass density is obtained from Eqs. (14) and (17) by setting $\xi(\mathbf{r}) = 1$; the result is

$$\rho(\mathbf{r}) = \frac{1}{J}\sum_j w(\mathbf{r}-\mathbf{r}_j). \tag{18}$$

Similarly, a continuous function approximating the entropy density $s = \rho S$ is obtained by setting $\xi(\mathbf{r}) = S(\mathbf{r})$, the specific entropy; the result is

$$s(\mathbf{r}) = \frac{1}{J}\sum_j S_j w(\mathbf{r}-\mathbf{r}_j). \tag{19}$$

From our earlier discussion, it follows that these approximations converge as $J \to \infty$ and $\sigma \to 0$.

Equations (4), (6), and (7) may be used to express ∇P and $\nabla\cdot\mathbf{F}$ in terms of space derivatives of the two state variables ρ and s, and these derivatives can now be expressed in terms of derivatives of w using Eqs. (18) and (19). In this way, approximations for ∇P and $\nabla\cdot\mathbf{F}$ are obtained for use in the difference equations discussed below.

Although the convergence of the approximations for ρ and s imposes no constraints on w additional to those given in Eqs. (15) and (16), the behavior of the scheme when J is not large can be improved by also insisting that w be non-negative and have continuous second derivatives. The non-negativity of w ensures that ρ and P are everywhere non-negative, and the continuity of its second derivatives ensures that $\nabla\cdot\mathbf{F}$ is a continuous function of position.

According to this continuous representation, the protostar occupies the volume made up of the points that lie within σ of at least one of the points $\mathbf{r}_j$. Now, since the assumed continuity of w requires that $w \to 0$ as $|\mathbf{r}-\mathbf{r}_j| \to \sigma$, it follows that $\rho \to 0$ as the surface of this volume is approached and, for $\gamma > 1$, this implies that $T \to 0$ also. The continuous representation therefore satisfies the boundary condition given in Eq. (9); consequently, it is automatically taken into account when space derivatives of state variables are calculated from Eqs. (18) and (19).

(*c*) *Difference Equations.* For the dynamical part of the calculation, we use the familiar time-centered, explicit scheme in which position and velocity are defined at alternate time steps. The difference equations approximating Eqs. (1) and (2) are then

$$\frac{\mathbf{v}_j^{n+1}}{(R^{n+1})^{1/2}} - \frac{\mathbf{v}_j^{n-1}}{(R^{n-1})^{1/2}} = \frac{(\Delta\tau)^n}{(R^n)^{1/2}}\left[-\frac{1}{\rho}\nabla P - \nabla\phi\right]_j^n, \tag{20}$$

$$R^{n+2}\mathbf{r}_j^{n+2} - R^n\mathbf{r}_j^n = (\Delta\tau)^n R^{n+1}\mathbf{v}_j^{n+1}, \tag{21}$$

where the notation $[\ ]_j^n$ indicates that the bracketed quantity is evaluated at time τ^n and position $\mathbf{r}_j$ using the continuous representation provided by Eqs. (18) and (19). The scale factor $R^n = R(\tau^n)$ is obtained by integrating Eq. (11) with initial condition $R(0) = 1$.

With the density given by Eq. (18), the solution of Poisson's equation is straightforward if w is chosen to be a function only of $|\mathbf{r}-\mathbf{r}'|$, for then the mass distribution becomes a superposition of spherically symmetric distributions, to each of which Newton's theorem applies. Accordingly,

$$\nabla\phi = \sum_k m(r)\frac{\mathbf{r}-\mathbf{r}_k}{r^3}, \tag{22}$$

where $r = |\mathbf{r}-\mathbf{r}_k|$ and

$$m(r) = \frac{4\pi}{J}\int_0^r w(x)x^2dx. \tag{23}$$

From Eqs. (15) and (16), it follows that $m(r) = 1/J$ for $r \geq \sigma$; consequently, $|\nabla\phi| \to |\mathbf{r}|^{-2}$ as $|\mathbf{r}| \to \infty$. The boundary condition on ϕ is therefore satisfied. Equations (22) and (23) allow $[\nabla\phi]_j^n$ to be calculated for use in Eq. (20).

The difference equation adopted as an approximation for Eq. (5) is

$$S_j^{n+2} - S_j^n = \frac{1}{2}(\Delta\tau)^n(H_j^{n+2} + H_j^n), \tag{24}$$

where

$$H_j^n = \lambda^n\{\nu + [-\nabla\cdot\mathbf{F}/\rho T]_j^n\}. \tag{25}$$

The derivative $d(\ln R)/d\tau$ has been eliminated using Eq. (11).

This difference equation is implicit and must be solved iteratively. The following procedure has proved successful: (1) A first estimate of S_j^{n+2} is obtained from the explicit difference equation

$$S_j^{n+2} - S_j^n = (\Delta\tau)^n H_j^n; \tag{26}$$

(2) the current estimate of S_j^{n+2} is used to calculate H_j^{n+2}, which is then substituted into Eq. (24) to obtain an improved estimate of S_j^{n+2}; (3) step (2) is repeated until convergence is achieved.

In the calculations reported later (Sec. IV), this iterative procedure (modified to include an 80% undercorrection factor) gives an accuracy of 0.0001 in S_j^{n+2} after about three to five iterations.

As initial values for these difference equations, the quantities $\mathbf{r}_j^0$, $\mathbf{v}_j^{-1}$, and S_j^0 must be specified for each of the J gas particles. The boundary conditions, as noted earlier, have been incorporated into the procedures for calculating $[\nabla P]_j^n$, $[\nabla\phi]_j^n$, and $[\nabla\cdot\mathbf{F}]_j^n$ from the continuous representations of ρ and s.

(*d*) *Broadening Function.* In addition to the conditions given in Eqs. (15) and (16), we have assumed that w is a non-negative function of the single variable $r = |\mathbf{r} - \mathbf{r}'|$ and has a continuous second derivative. A function satisfying all these conditions is

$$w = \frac{105}{16\pi}\frac{1}{\sigma^3}(1 + 3z)(1 - z)^3 \tag{27}$$

for $z = r/\sigma \leq 1$ and $w = 0$ for $z > 1$. This bell-shaped function is such that $w(r) = \frac{1}{2}w(0)$ for $r = 0.386\sigma$.

With such a simple choice for w, the quantities ∇w and $\nabla^2 w$ required in the calculation of ∇P and $\nabla\cdot\mathbf{F}$ can be evaluated analytically, as can $m(r)$.

(*e*) *Stability.* The explicit difference scheme for computing the motions of the gas particles [i.e., Eqs. (20) and (21)] should be stable if $\Delta\tau$ is small compared to the minimum characteristic time scale for the motion of any one particle. When the scheme is representing a gas—that is, before significant collisional relaxation has occurred [see Sec. II (g)]—this minimum time scale is the oscillation period associated with the passage of a sound wave of the maximum wave number $k_{\max}$ permitted by the scheme's spatial resolution. Accordingly, since $k_{\max} \simeq 1/\sigma$, we expect stability when, for every particle, $2\pi\sigma/c_s \gg \Delta\tau$, where c_s is the local adiabatic speed of sound. The stability criterion should therefore be

$$(\Delta\tau)^n < (\Delta\tau)_*^n = \min_{(j)}\left\{\frac{\alpha\sigma}{[c_s]_j^n}\right\}, \tag{28}$$

where α is a number $\simeq 1$ whose precise value depends on the shape of w. Not surprisingly, this stability criterion has the form of a Courant condition on the time step.

The value of α appropriate for the broadening function given in Eq. (27) has been approximately determined by the following numerical experiment: Adiabatic (i.e., $S_j^0 = S$) stellar models in hydrostatic equilibrium [see Sec. II (h)] were perturbed, and the isentropic evolution (i.e., $S_j^{n+2} = S_j^0$) of the perturbation followed using Eqs. (20) and (21) with scale factor $R(\tau) \equiv 1$ and time step $(\Delta\tau)^n = (\Delta\tau)_*^n$. For a given model, such integrations do indeed reveal instability when α is greater than a certain critical value. This critical value is, however, somewhat model dependent. Moreover, the abruptness of the onset of instability becomes less marked for models with smaller values of $J\sigma^3$—such models are of course poorer representations of a continuum.

The following results are typical: For a $\gamma = 5/3$ adiabat ($n = 3/2$) of unit radius ($S = -1.2862$) with $J = 100$ and $\sigma = 0.6$, instability is found for $\alpha > 0.75$. For a $\gamma = 3$ adiabat ($n = 1/2$) of unit radius ($S = 0.4622$) with $J = 80$ and $\sigma = 0.7$, instability is found for $\alpha > 0.59$. This model dependence is probably a consequence of $k_{\max}$ not greatly exceeding unity, which implies that the particles are responding not to sound waves but to pulsations in low-order modes.

The thermal histories of the gas particles are determined by Eq. (5), which, if $\nabla\cdot\mathbf{F}$ is expressed in terms of derivatives of state variables, becomes the equation of heat conduction with the addition of lower-order terms. The stability of difference equations for the equation of heat conduction is, however, known to be practically unaffected by such terms (Richtmeyer and Morton 1967, p. 195); consequently, our knowledge of the stability criteria for the various schemes (Richtmeyer and Morton 1967, p. 189) can be used to anticipate (1) that the centered, implicit scheme given in Eq. (24) will be unconditionally stable and (2) that the uncentered, explicit scheme given in Eq. (26) will be stable if $(\Delta\tau)^n < (\Delta\tau)_+^n$, where

$$2(\gamma - 1)\lambda^n \max_{(j)}\left\{\left[\frac{T^3}{\rho^2}\right]_j^n\right\}\frac{(\Delta\tau)_+^n}{(\beta\sigma)^2} = 1. \tag{29}$$

As with α in the Courant condition, β is a number $\simeq 1$ whose precise value depends on the shape of w.

Because the explicit scheme was used during the development of this numerical technique, the value of β appropriate for the broadening function given in Eq. (27) was also determined by numerical experiment. In these experiments, the radiative cooling of static (i.e., $\mathbf{r}_j^{n+2} = \mathbf{r}_j^0$) stellar models was computed using Eq. (26) with $(\Delta\tau)^n = (\Delta\tau)_+^n$. Such integrations reveal instability when $\beta > 0.35$, a critical value having little dependence on the model; Eq. (29) with $\beta = 0.35$ therefore determines the maximum stable time step for Eq. (26).

The expectation that Eq. (24) is unconditionally stable is not contradicted by the available numerical results. Stability for time steps significantly exceeding $(\Delta\tau)_+^n$ cannot be tested, however, since the convergence of the iterative procedure [Sec. II (c)] for obtaining S_j^{n+2} then becomes very slow.

The above results show that the stability criteria for this finite-size particle scheme have the same form as

those for conventional difference equations. The mesh size Δx in conventional criteria is simply replaced by a length that is approximately the half-width of the function w.

(*f*) *Bulk Viscosity.* Because of the nonadiabicity of motions in its outer envelope, pulsations of the protostar are damped on time scales short compared to the contraction time scale. Unfortunately, this characteristic is not shared by a model having a feasible number of particles since, with particles distributed according to mass density, none are to be found in the outer envelope [see Sec. III (a), Fig. 1]. The consequence of this near absence of damping is a slow buildup of acoustic energy, since both integration errors and the accelerated contraction [Sec. IV (a)] are sources of acoustic disturbance. In order to prevent this, a viscous pressure term is added to the scheme.

The viscous pressure is taken to be

$$Q = -\epsilon\sigma\rho c_s \nabla \cdot \mathbf{u}, \tag{30}$$

where

$$\mathbf{u} = \mathbf{v} - \frac{d\ln R}{d\tau}\mathbf{r} \tag{31}$$

is the velocity with respect to the contracting coordinate system. From Eqs. (11) and (31), it then follows that

$$\nabla \cdot \mathbf{u} = \nabla \cdot \mathbf{v} + (3\nu\lambda/\chi). \tag{32}$$

In order to calculate $\nabla\cdot\mathbf{v}$, we follow our earlier procedure and adopt

$$\rho\mathbf{v} = \frac{1}{J}\sum_j \mathbf{v}_j w(\mathbf{r} - \mathbf{r}_j) \tag{33}$$

as a continuous representation of the momentum density. Combined with Eq. (18), this gives a continuous representation of the velocity, from which $\nabla\cdot\mathbf{v}$ may be calculated. With the further approximation of replacing $[\mathbf{v}]_k$ by $\mathbf{v}_k$, the resulting expression for $\nabla\cdot\mathbf{v}$ at particle position $\mathbf{r}_k$ is

$$[\nabla \cdot \mathbf{v}]_k = \frac{\sum_j (\mathbf{v}_j - \mathbf{v}_k) \cdot (\nabla w)_{jk}}{\sum_j (w)_{jk}}. \tag{34}$$

Because the desired quantity is ∇Q, a continuous representation of Q is required. Accordingly, again following the earlier procedure, we take

$$Q(\mathbf{r}) = \frac{1}{J}\sum_k [Q/\rho]_k w(\mathbf{r} - \mathbf{r}_k), \tag{35}$$

where $[Q/\rho]_k$ is calculated from Eqs. (30), (32), and (34). The quantity $\rho^{-1}\nabla Q$ is then readily calculated at the position of each particle and the result included in the right-hand side of Eq. (20).

The viscous pressure gradient derived in this way is not properly centered when included in Eq. (20) since it is calculated using velocities at time τ^{n-1}. This failure is, however, shared by a widely used one-dimensional Lagrangian scheme (Richtmeyer and Morton 1967, p. 318).

The energy dissipated by this viscous term is not returned to the system by means of a heating term in Eq. (25) since, for the real protostar, the dissipation occurs in the outer layers. This heating term is of course necessary when the purpose of the viscous pressure is to treat shock formation.

(*g*) *Collisional Relaxation.* The technique described above may be regarded as an analog for gas dynamics of the finite-size particle schemes used in stellar dynamics and plasma physics (see, e.g., Dawson 1972). As for such schemes, therefore, we can anticipate that, as an integration advances, particle encounters will have an increasingly deleterious effect on the results. Clearly, when most particles have undergone significant deflections due to encounters, the calculation will no longer be relevant to the gas dynamical problem being investigated.

The overlapping of the finite-size particles produces continuous, but somewhat bumpy, distributions of mass and specific entropy; the force fluctuations resulting from this bumpiness cause the deflections. The effect of encounters may therefore be diminished by increasing either J or σ, since the result, in both cases, is a smoother gaseous configuration. Accordingly, the useful duration of an integration may be extended by using more computer time (increasing J) or by sacrificing spatial resolution (increasing σ).

Because of collisional relaxation, the error of a calculation with this technique will not remain bound as $\tau \rightarrow \infty$. [For example, if a stellar model close to hydrostatic equilibrium is integrated forward in time without radiative cooling (i.e., $\lambda \equiv 0$), it does not remain close to hydrostatic equilibrium indefinitely. A slow buildup of kinetic energy in particle motions occurs and this eventually leads to particle loss to infinity.] Within a specified finite interval of time, however, we may anticipate that a solution of specified accuracy can always be obtained by choosing σ small enough to provide adequate spatial resolution and J large enough to limit the effects of encounters.

(*h*) *Initial Models.* Because Monte Carlo theory has been used in the derivation of this technique, the initial particle positions should ideally be a random sample from the mass distribution of the initial configuration. For feasible values of J, however, the resulting sampling errors in the number density of particles are not small. As a result, the forces acting on the particles have large deviations from their expected values and these deviations give rise to violent motions that dominate the effects being investigated.

This problem also arises for the analogous plasma physics codes, where it is overcome by suppressing sta-

tistical fluctuations to such a degree that a quiet start to an integration is obtained (Dawson 1972, p. 319). For this technique, the following procedure has been used to generate adiabatic stellar models that yield quiet starts:

A set of particle positions $\mathbf{r}_j^0$ is chosen randomly and we set $S_j^0 = S$ and $\mathbf{v}_j^{-1} = \mathbf{0}$. This model is then integrated forward in time using the difference equations

$$\mathbf{v}_j^{n+1} = \left\{ \mathbf{v}_j^{n-1} + \Delta\tau \left[-\frac{1}{\rho}\nabla P - \nabla\phi \right]_j^n \right\} \Big/ (1+\delta), \tag{36}$$

$$\mathbf{r}_j^{n+2} = \mathbf{r}_j^n + (1+\delta)\Delta\tau \mathbf{v}_j^{n+1}, \tag{37}$$

and

$$S_j^{n+2} = S_j^n. \tag{38}$$

With $\delta > 0$, the factor $(1+\delta)$ damps the motions arising from the sampling errors in the initial model; consequently, after $\simeq 5$ pulsation periods (with $\delta = 0.3$), a solution is obtained in which, to a good approximation, the force on each particle vanishes. The resulting particle positions then give a quiet start when used as initial conditions for Eqs. (20), (21), and (24).

By including centrifugal force in such a calculation, models for rotating adiabatic stars are readily obtained.

A model obtained with the above technique is typically far more accurate than one in which the particles are randomly distributed. Improving the precision of an estimator by departing from random sampling is, in fact, standard Monte Carlo practice. An example is the technique of stratified sampling (Hammersley and Handscomb 1964), for which the gain in precision derives, as in our case, from a reduction in the statistical fluctuations of the number density of quadrature points.

(*i*) *Related Techniques.* Particle schemes for gas dynamical problems of astronomical interest have recently been described by Gott and Thuan (1976) and by Lin and Pringle (1976). Both of these schemes were devised for pressure-free, viscous flows; they are therefore not applicable to the slow, pressure-controlled contraction of a protostar. Nevertheless, the work of Lin and Pringle was the direct stimulus of the present investigation.

More closely related to the scheme described herein is the particle-in-cell (PIC) method developed at Los Alamos (Harlow 1964). In the PIC method, however, the particles' momentum changes are due not only to the action of forces but also to a momentum sharing that occurs in each cell after each time step—a process that effectively introduces a coefficient of viscosity large enough to spread shocks over several cell widths. In a three-dimensional calculation of low resolution, this numerical viscosity would be prohibitively large, as also would be the numerical heat conduction that arises from the corresponding sharing of internal energy.

Prendergast's "beam" scheme (Sanders and Prendergast 1974) would also be expected to suffer from large transport coefficients if used for a three-dimensional calculation of low resolution.

III. TESTS

With a view to demonstrating the merits of this finite-size particle scheme, we now test its ability to solve hydrostatic and hydrodynamic problems for stars. Because preliminary fission calculations showed no significant departures from symmetry about the invariable plane, symmetry about the x,y plane is imposed for all the calculations reported below and in Sec. IV. The difference equations are therefore used to compute the changes in $\mathbf{r}_j$, $\mathbf{v}_j$, and S_j for half of the particles, the changes for the remaining half being such as to preserve symmetry.

(*a*) *Hydrostatics.* As a first test, we apply the technique of Sec. II (h) to obtain an equilibrium model for a nonrotating $n = 3/2$ polytrope of unit radius. The parameters are $J = 60$, $\sigma = 0.6$, $\gamma = 5/3$, and $S_j = -1.2862$ for all j.

In Fig. 1, the values of $\log \rho$ and $-\rho^{-1}\nabla\cdot\mathbf{F}$ at the positions of the 30 particles with $z > 0$ are plotted against distance from the center of mass. Results of an essentially exact one-dimensional calculation are also shown.

Inspection of the log ρ values reveals very good agreement with the exact solution. In particular, the

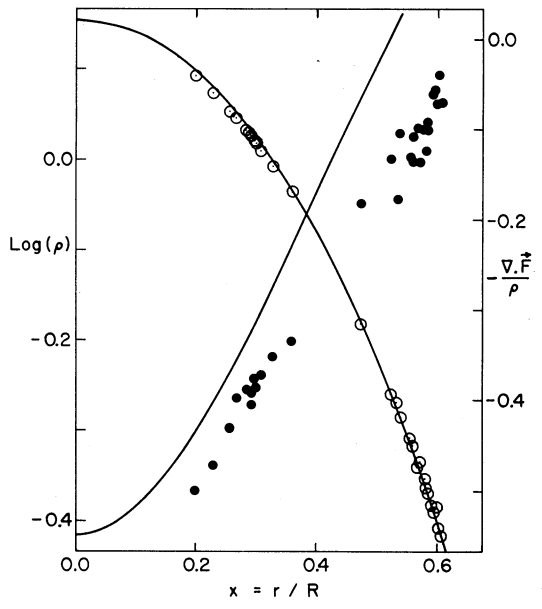

FIG. 1. Structure of $n = 3/2$ polytrope. Log ρ (*open circles*) and $-\rho^{-1}\nabla\cdot\mathbf{F}$ (*filled circles*) are plotted against distance from center of mass.

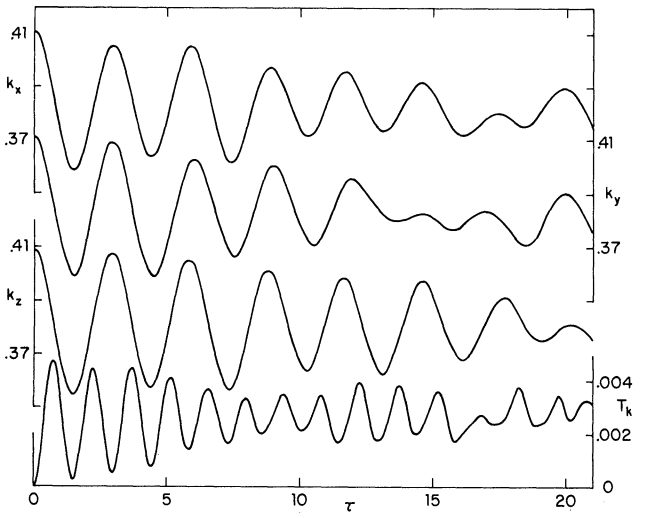

FIG. 2. Oscillations of $n = 3/2$ polytrope. Radii of gyration k_x, k_y, k_z and kinetic energy T_k are plotted against time τ for model with $J = 40$ and $\sigma = 0.6$.

small vertical scatter implies that departures from spherical symmetry are slight. Thus, starting with random particle positions, the code is able to discover that, in the absence of angular momentum, a star must be spherically symmetric. This is an important test of the scheme's representation of gas pressure.

Inspection of the values of $-\rho^{-1}\nabla\cdot\mathbf{F}$ reveals greater vertical scatter and poorer agreement with the exact solution. Poorer results are of course to be expected for this quantity since it requires that the slightly bumpy continuous representations of ρ and s [i.e., Eqs. (18) and (19)] be differentiated twice. Nevertheless, the values of $-\rho^{-1}\nabla\cdot\mathbf{F}$ are still such that the interior of the model is cooling relative to the exterior; consequently, its secular evolution would indeed be contraction to a more centrally condensed structure.

The accuracy of the solution has been tested at the particles' positions because this determines the success of time-dependent calculations. The continuous representation can, however, also be used to test a model's properties throughout its structure. Such tests for static and rotating polytropes are reported by Gingold and Monaghan (1977) with excellent results.

(*b*) *Hydrodynamics.* As a further test of the scheme's representation of pressure, we now study the propagation of disturbances. To do this, we attempt to compute spherical, isentropic pulsations of polytropic models with $n = 3/2$ and $\gamma = 5/3$.

Using the technique of Sec. II (h), we first determine the equilibrium positions $\mathbf{r}_j$ of the J particles. The initial conditions for the dynamical calculation are then taken to be $\mathbf{v}_j^{-1} = \mathbf{0}$, $S_j^0 = -1.2862$, and $\mathbf{r}_j^0 = [1 + 0.1\xi(|\mathbf{r}_j|)]\mathbf{r}_j$, where ξ is the eigenfunction of the fundamental radial mode, normalized so that $\xi(1) = 1$. (A tabulation of ξ was kindly provided by A. Cooper.) This model is then integrated forward in time using Eqs. (20), (21), and (24) with $\lambda(\tau) \equiv 0$.

Results for a model with $J = 40$ and $\sigma = 0.6$ are shown in Fig. 2. Radii of gyration in three perpendicular directions (computed on the assumption that the particles are point masses) are plotted against time in the upper part of this diagram. We see that only for $\tau \lesssim 10$ does the motion approximate the expected spherical pulsations of constant amplitude. At later times, large departures from sphericity are evident.

Particle encounters are, of course, responsible for these disappointing results [see Sec. II (g)]. Their effect, on average, is to introduce increasing departures from each particle's expected motion, which is a purely radial oscillation with constant amplitude and period. For the model as a whole, this implies a diversion of energy from the fundamental radial mode to other modes, both radial and nonradial. Because this is not a dissipative effect, the resulting decay of the fundamental mode should not correspond to a decay of the time-averaged kinetic energy. This expectation is confirmed by the time variation of kinetic energy shown in the lower part of Fig. 2. (The time-averaged kinetic energy actually increases slowly with time at the expense of gravitational energy as the system tries to approach a relaxed state.)

From the discussion of Sec. II (g), we expect that increasing either J or σ will extend the interval over which spherical pulsations can be followed. As an illustration of this, Fig. 3 shows the result of repeating the above experiment with J increased from 40 to 100. A dramatic improvement is evident.

Because of the scheme's poor representation of the outer layers of centrally condensed stars [see Sec. II (f) and Fig. 1], accurate pulsation periods are not to be expected. Nevertheless, the results in Fig. 3 yield the estimate $P = 3.40$ for the fundamental period, which compared favorably with the exact value 3.82.

(*c*) *Numerical Fission?.* The above time-dependent calculations involve neither rotation nor radiative losses.

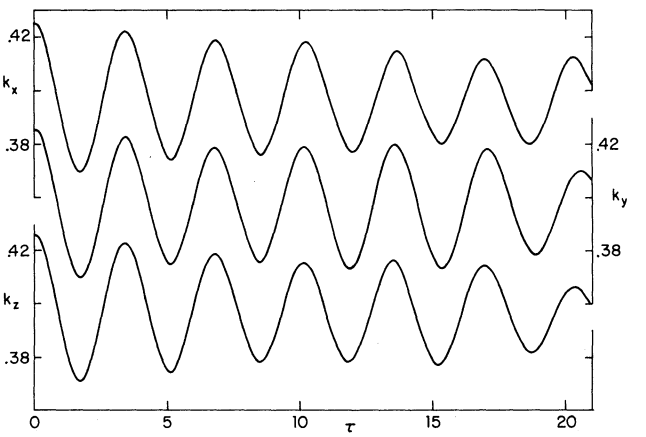

FIG. 3. Oscillations of $n = 3/2$ polytrope. Radii of gyration k_x, k_y, and k_z plotted against time τ for model with $J = 100$ and $\sigma = 0.6$.

Without further tests, therefore, a calculation showing fission might well be doubted on the grounds that fission may be an artifact of the scheme's treatment of these effects. Accordingly, we now carry out tests to see if the inclusion of either effect leads to fission. In the first test, the motion of a rotating star is followed with radiative losses suppressed. In the second test, the motion of a nonrotating star is followed with radiative losses permitted.

For the first test, an equilibrium model of a uniformly rotating $n = 3/2$ polytrope was obtained using the technique of Sec. II (h). The parameters are $J = 140$, $\sigma = 0.7$, $\gamma = 5/3$, $S_j = -1.2862$ for all j, and the angular velocity $\Omega = 0.54$. As in the pulsation calculation, the motion (i.e., the rotation) of this model was then computed using Eqs. (20), (21), and (25) with $\lambda(\tau) \equiv 0$.

In reporting the results of this test, it is convenient to represent the model's dimensions and shape in terms of the semimajor axes a, b, and c of the homogeneous ellipsoid whose moments of inertia about its principal axes are identical to those of the model. Represented in this way, the initial model has dimensions $a = 0.773$, $b = 0.761$, and $c = 0.579$. These results show the marked rotational flattening to be expected for $\Omega = 0.54$; they are also consistent with negligible departures from axial symmetry. The motion of this model was followed for 5.2 rotation periods ($\tau = 60$), and during this time the range of variation was 0.773–0.790 for a, 0.759–0.773 for b, and 0.570–0.580 for c. The model therefore preserves its shape and dimensions rather accurately; no tendency to fragment is apparent and no particles are lost.

Conservation of angular momentum was also checked. Calculated on the assumption that the particles are point masses, this quantity meanders between 0.1266 and 0.1272—i.e., constancy to ±0.2%.

For the second test, an equilibrium model of a nonrotating $n = 3/2$ polytrope was obtained with parameters $J = 140$, $\sigma = 0.7$, $\gamma = 5/3$, and $S_j = -1.2862$ for all j. The motion that results from setting $\lambda(\tau) \equiv 0.8$ was then calculated, the initial velocities being $\mathbf{v}_j^{-1} = \mathbf{0}$.

The quantity $\zeta = (a - c)/(a + c)$ is a convenient measure of the departures from sphericity that arise during the contraction. From its initial value of 0.002, ζ reaches a high of 0.29 at $\tau = 18$ and averages 0.12 during an integration to $\tau = 56$. Thus, non-negligible departures from sphericity do indeed occur. The model does not fragment, however, and only for a brief interval is one pair of particles detached.

This second test and the values of $-\rho^{-1}\nabla\cdot\mathbf{F}$ plotted in Fig. 1 show that the treatment of radiative conductivity is not one of the scheme's strong points. These mediocre results are, however, a consequence of the need to evaluate second derivatives; a simple remedy is, therefore, not likely.

For $\nabla\cdot\mathbf{F}$ to be a smooth function of position, many finite-size particles must overlap at a typical point in a model. Accordingly, for problems involving radiative conduction, the lower limit on σ (given J) is likely to be determined by the need to limit the dynamical consequences of the fluctuations in $\nabla\cdot\mathbf{F}$, rather than to limit the effects of particle encounters [Sec. II (h)].

IV. FISSION

In the belief that the above tests have demonstrated the scheme's utility even at low resolution, we now use it to study the contraction of a rotating protostar.

(*a*) *The Ideal Problem and its Modification.* Ideally, perhaps, one would wish to start with a uniformly rotating $n = 3/2$ polytrope—i.e., a fully convective Hayashi star. This model's slow, Kelvin–Helmholtz contraction to a differentially rotating and more centrally condensed configuration would then be followed to the point of dynamical overstability to the growth of a nonaxisymmetric perturbation (Bodenheimer and Ostriker 1970). Finally, the ensuing rapid evolution would be followed and the fission hypothesis thereby tested.

Unfortunately, this ideal problem poses two serious practical difficulties for the scheme described in Sec. II. The first is the obvious impossibility of computing Kelvin–Helmholtz contraction with a code whose time step is limited by the Courant condition [Eq. (28)]. The second difficulty is the need for high spatial resolution as the model becomes very centrally condensed ($n \simeq 3$).

Fortunately, these difficulties can be overcome by suitably modifying the ideal problem. The time-step difficulty is eliminated by speeding up the contraction, and this is done by choosing λ in Eq. (5) to be such that the ratio of the thermal and dynamical time scales is $\simeq 5$ instead of 10^6–10^{10}. Provided the contraction remains sufficiently slow for the point of instability to be reached with rotation accounting for most of the kinetic energy, the results may reasonably be regarded as pertaining to the fission problem for optically thick protostars undergoing quasistatic contraction and not to the fragmentation problem for optically thin protostars undergoing free-fall collapse.

The difficulty with spatial resolution is overcome by increasing γ from 5/3 to 3; the initial adiabatic model is then the less centrally condensed $n = 1/2$ polytrope. This change allows a greater amount of rotational kinetic energy (relative to gravitational energy) to be stored in the uniformly rotating initial model, and this implies that less evolution in the direction of increasing central condensation suffices to bring the model to the point of instability.

Neither of these modifications changes the problem's mathematical character. Such an assertion cannot be made with regard to the inclusion of a viscous pressure term [Sec. II (f)], however.

(*b*) *A Particular Case.* Details of the evolutionary sequence for one model will now be used to illustrate the application of the scheme to the fission problem.

The parameters are $J = 300$, $\sigma = 0.55$, $\gamma = 3$, $\epsilon = 0.25$ [Eq. (30)], and the contraction results from setting $\lambda(\tau) \equiv 0.8$. The initial particle positions $\mathbf{r}_j^0$ are from an equilibrium model [Sec. II (h)] of a uniformly rotating $n = 1/2$ polytrope with $\Omega = 0.54$, and the initial velocities $\mathbf{v}_j^{-1}$ corresponding, in the contracting coordinate system, to solid body rotation with this angular velocity. The initial specific entropies $S_j^0 = 0.4622$ for all j are such that the model would have unit radius in the absence of rotation.

With these choices, the initial rotation period is 11.6, the initial pulsation period (neglecting rotation) is $\simeq 2.4$ and, from Eq. (11), the Kelvin–Helmholtz time scale for the homologously contracting spherical model is $\chi/\nu\lambda = 12.2$. Initially, therefore, the e-folding time for the contraction of the coordinate system corresponds approximately to one rotation period and to five pulsation periods.

For the early evolution of the model, it is useful to detect departures from axial symmetry by again calculating the major axes of the equivalent homogeneous ellipsoid [see Sec. III (c)] and to monitor the approach to instability by calculating $t_R = T_R/|W|$, where

$$T_R = (1/2J) \sum_j (-y_j u_j + x_j v_j)^2/(x_j^2 + y_j^2) \quad (39)$$

is the rotational kinetic energy and W is the gravitational energy, which is evaluated with the quadrature formula,

$$W = -(1/J) \sum_j \mathbf{r}_j \cdot [\nabla\phi]_j. \quad (40)$$

The quantity $t_K = T_K/|W|$, where T_K is the total kinetic energy, is also useful, since $(t_K - t_R)/t_R$ is a measure of departures from purely rotational motion. (In calculating kinetic energies and the angular momentum, the velocity of a particle at time τ^n is obtained by averaging its velocities at times τ^{n-1} and τ^{n+1}.)

For the initial model, the above quantities are $a = 1.091$, $b = 1.086$, $c = 0.700$, $t_R = 0.121$, and $t_K = 0.125$.

From the work of Lynden-Bell (1964), Bodenheimer and Ostriker (1970), and Lebovitz (1972), we expect a rotating protostar with sufficient angular momentum to contract through a sequence of axially symmetric configurations until it becomes dynamically overstable to the growth of a nonaxisymmetric mode when $t_R \simeq 0.26$. Because *shear* viscosity is probably intrinsic to the numerical scheme, the model will approximate a protostar's expected behavior only if the speeded-up contraction is fast enough to prevent significant growth of departures from axial symmetry during the time that $0.14 < t_R < 0.26$. On the other hand, the contraction must be slow enough to approximate quasistatic contraction for $t_R < 0.26$. Fortunately, these requirements turn out not to be mutually exclusive. The model reaches $t_R = 0.26$ at $\tau = 14.6$ with $a = 1.567$, $b = 1.443$, $c = 0.474$, and $(t_K - t_R)/t_R = 0.069$; the departure from axial symmetry is therefore slight, and rotation accounts for most of the total kinetic energy.

One unsatisfactory aspect revealed by the above data at $t_R = 0.26$ is the lack of resolution in the z direction. The reduction of c from 0.700 at $\tau = 0.0$ to 0.474 at $\tau = 14.6$ makes it comparable to the minimum resolved length, which is $\simeq 0.3$ for $\sigma = 0.55$. The subsequent models also suffer from inadequate resolution in the z direction.

That departures from axial symmetry appear prior to $t_R = 0.26$ indicates that the numerical scheme does indeed effectively introduce *shear* viscosity. A further indication of this is the significant redistribution of angular momentum that also occurs prior to $t_R = 0.26$. At this point, the average change since $\tau = 0$ of a particle's angular momentum is 36% of a particle's average angular momentum. {Note that the artificial *bulk* viscosity [Sec. II (f)] does not redistribute angular momentum and does not, therefore, contribute to secular instability at $t_R \simeq 0.14$ (Ostriker 1970)}

In the above discussion, $t_R = 0.26$ has been used to determine the onset of dynamical overstability, and this is justified by the finding of Ostriker and his coworkers (see Ostriker 1970) that this is rather accurate for polytropes of various n. Greater precision in locating this point cannot be achieved with this code because of the zero initial growth rate of the dynamical instability, the accelerated contraction, and the prior growth of departures from axial symmetry due to the secular instability at $t_R \simeq 0.14$.

The model's evolution subsequent to the onset of instability is illustrated by the six diagrams of Fig. 4, each of which is a plot of particle positions projected on the x,y plane—each point therefore represents two particles. Consecutive diagrams are separated by 30 time steps with $\Delta\tau = 0.2$, and the direction of rotation is anticlockwise.

In order to describe these results, it is useful to define a *component* to be a set of particles comprising all particles within distance σ of at least one other member of the set. If a component contains N particles, its mass will be referred to as Np; the term *debris* will be used to denote the totality of particles belonging to components with mass less than $10p$.

Defined in this way, a component is such that a pressure wave can propagate from any one of its member particles to any other member, but not to any nonmember. The sorting of the J particles into components with this definition is therefore a sensible way of detecting the presence of distinct model stars. Initially, there is of course just one component of mass $300p$ and no debris.

Using these definitions, we now briefly describe the structural changes shown in Fig. 4.

At $\tau = 22$, the principal component, which deviates significantly from axial symmetry, has mass $274p$. The remaining mass, $26p$, is in the form of debris.

At $\tau = 28$, the principal component has mass $254p$, its

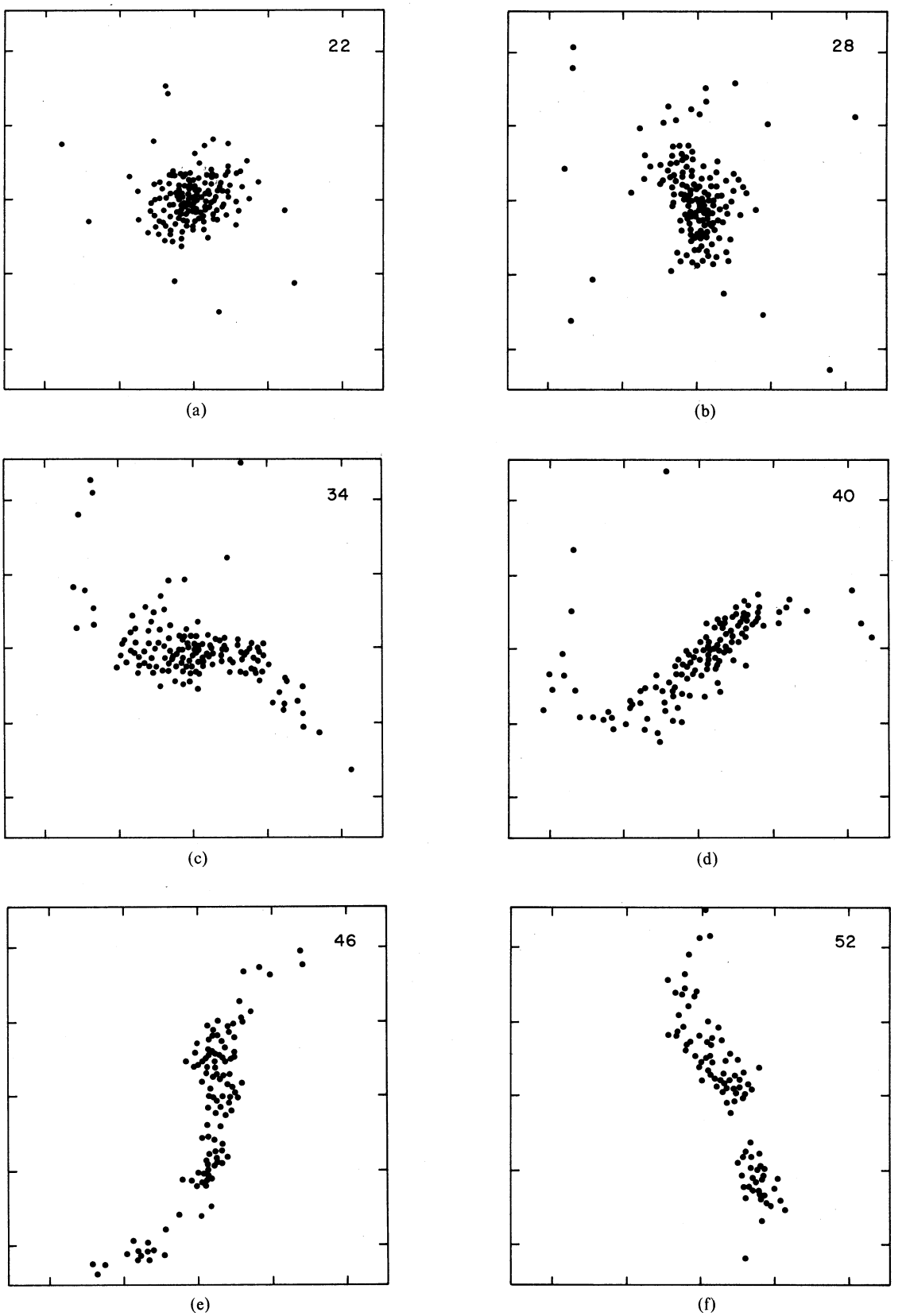

FIG. 4. Evolution of rotating protostar. Structure projected on equatorial plane is shown at the indicated times. Because of symmetry, each point represents two particles. The axes are marked at 5-σ intervals.

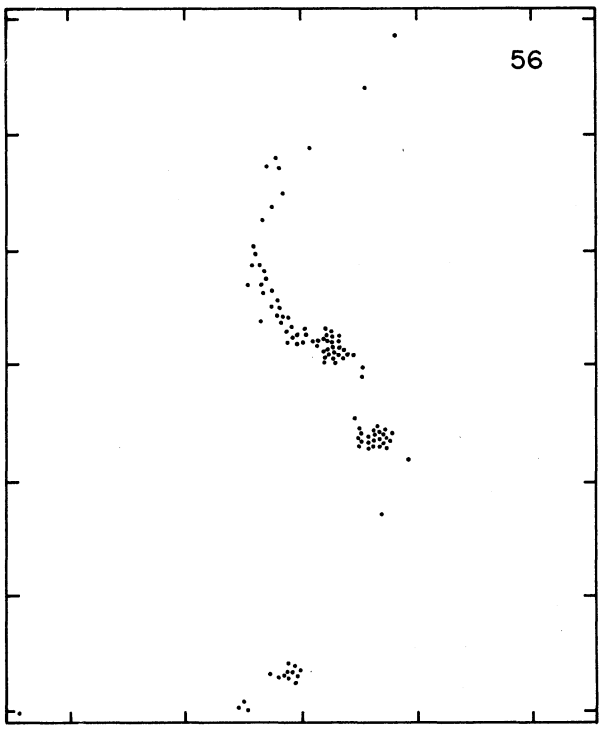

FIG. 5. Projected structure at $\tau = 56$. The axes are marked at 10-σ intervals.

departure from axial symmetry has increased, and a fore-to-aft asymmetry is evident. This latter effect suggests that a third-harmonic instability arises shortly after the onset of the second-harmonic instability that causes the initial departure from axial symmetry.

At $\tau = 34$, the principal component has mass $232p$ and there is a secondary component of mass $18p$ in the loose grouping of particles to the right of the principal component. This secondary component is short lived, however.

At $\tau = 40$, the principal component has mass $220p$ and it is now bar shaped. In the loose grouping of particles to the left of the principal component, there is a component of mass $26p$. With some loss of mass, this component survives to the end of the calculation.

At $\tau = 46$, the principal component has mass $176p$ and fission is clearly imminent. At the bottom of this diagram is the component formed at $\tau \simeq 40$. It is now well defined and has mass $20p$.

At $\tau = 52$, the principal component in the previous diagram has now fissioned into components of mass $112p$ and $58p$. Because of the contraction of the coordinate system, the component formed at $\tau \simeq 40$ has moved off the diagram, but it survives and has mass $20p$.

On a reduced scale, Fig. 5 shows the configuration of the system when the calculation ends at $\tau = 56$ with a further fission about to happen. The masses of the components at this time are $102p$, $56p$, and $22p$; they therefore comprise 60% of the original mass.

Because energy generation by nuclear burning was omitted, the contraction and the resulting fissioning continue indefinitely. Clearly, if energy generation had been included, the model could have been scaled so that the onset of nuclear burning stopped the contraction with the formation of a binary ($\tau \simeq 40$) or a triple system ($\tau \simeq 50$).

(*c*) *Variation of Parameters.* Because the main purpose of this section is to demonstrate that this finite-size particle scheme does indeed render the fission problem amenable to direct investigation by numerical calculation, the details of other cases will not be described here. Some of their general features are worth reporting, however.

The most important point to emphasize is the lack of robustness of the results. In other words, small changes in parameters do not always give small changes in the results. To some degree, this is a consequence of integrating through an instability—changing a parameter changes the preexisting perturbation that is amplified. A more important effect, however, seems to arise because gravitational torques between the debris and the main component (i.e., before fission) significantly influence the latter's evolution. This evolution is then sensitive to parameter changes because they result in a different set of particles becoming debris.

Despite this lack of robustness, the following general trends emerge from the numerous cases that have been computed:

(1) Following the appearance of departures from axial symmetry, a substantial fraction of the mass is nearly always lost as debris. Because debris is not formed when either radiative losses or rotation are suppressed [Sec. III (c)], this effect is probably real and not numerical, though its magnitude may well be affected by the poor representation of surface layers. The formation of debris is presumably due to the transfer of angular momentum from the protostar's interior to its surface by the action of gravitational torques.

(2) Evolution into a bar-shaped structure is common—the losses of angular momentum to the debris rarely stops this.

(3) If fission does occur, it leads to a binary of small mass ratio, typically towards the lower end of the range 0.1–0.5.

V. DISCUSSION

The main purpose of this paper has been to describe and test a numerical scheme that can be applied to two- and three-dimensional gas dynamical problems of astronomical interest. The tests reported in Sec. III show that the scheme behaves well even when used with low spatial resolution; it can therefore be applied to three-dimensional problems using present-day computers. (The usefulness of such calculations depends, however, on there being a significant question that is not known *a priori* to be unanswerable at low resolution.) The en-

couraging results obtained by applying this scheme to the fission problem have been described in Sec. IV. Its application to the two-dimensional gas flow in the plane of a barred spiral is described by Sanders (1977). Also, as noted earlier, Gingold and Monaghan (1977) have described experiments, similar to those of Sec. III (a), that test the scheme's ability to reproduce static and rotating stellar models.

With regard to the fission problem, perhaps all that can be safely claimed on the basis of the present results is that our belief in fission as the formation mechanism for close binaries is strengthened. A stronger statement is inadvisable in view of the low spatial resolution and the various necessary modifications of the ideal problem. In particular, it may be premature to conclude that fission always yields binaries with small mass ratios. Nevertheless, because this aspect of the present calculations is in apparent contradiction with the existence of close binaries having mass ratios $\simeq 1$, it is worthy of further discussion. The point to be made in this regard is that, following fission, we may reasonably expect the binary to be a contact system and that only after further evolution on a thermal time scale can it become a detached binary. Because significant mass exchange may occur during this contact phase (Lucy 1976), the mass ratio immediately following fission may have little relevance to observed mass ratios. Such an effect cannot be investigated with this scheme because of its poor representation of the outer layers of the components.

The computing time for the calculation described in Sec. IV (b) was 4.4 min on an IBM 360/95. Because the computing time per step is $\propto J^2$, calculations with $J \sim 500$–1000 are the upper limit of what is possible with this code on this computer, and such calculations are planned after testing some possible improvements in the scheme. The gain in spatial resolution will be slight, however, since σ cannot be reduced faster than $J^{-1/3}$. For a significant gain in resolution, the scheme must be combined with an efficient Poisson-equation solver.

The bulk of this research was done during a sabbatical leave spent at Cambridge and Geneva. I am grateful to M. Rees, D. Lynden-Bell, and L. Woltjer for making these visits possible. I also wish to acknowledge useful discussions with E. Graham and K. H. Prendergast. This work has been partially supported by NSF grant AST 76-08917; a grant of computer time at the Goddard Institute for Space Studies is also gratefully acknowledged.

REFERENCES

Bodenheimer, P., and Ostriker, J. P. (1970). Astrophys. J. **161,** 1101.
Chandrasekhar, S. (1969). *Ellipsoidal Figures of Equilibrium* (Yale U. P., New Haven).
Dawson, J. M. (1972). *Gravitational N-Body Problem,* edited by M. Lecar (Reidel, Dordrecht), p. 315.
Gingold, R. A., and Monaghan, J. J. (1977). Mon. Not. R. Astron. Soc. To be published.
Gott, J. R., III, and Thuan, T. X. (1976). Astrophys. J. **204,** 649.
Hammersley, J. M., and Handscomb, D. C. (1964). *Monte Carlo Methods* (Methuen, London).
Harlow, F. H. (1964). *Methods in Computational Physics,* edited by B. Alder, S. Fernbach, and M. Rotenberg (Academic, New York), Vol. 3.
James, R. A. (1964). Astrophys. J. **140,** 552.
Lebovitz, N. R. (1972), Astrophys. J. **175,** 171.
Lebovitz, N. R. (1974). Astrophys. J. **190,** 121.
Lin, D. N. C., and Pringle, J. E. (1976). *Structure and Evolution of Close Binary Systems,* edited by P. Eggleton, S. Mitton, and J. Whelan (Reidel, Dordrecht), p. 237.
Lucy, L. B. (1976). Astrophys. J. **205,** 208.
Lynden-Bell, D. (1964). Astrophys. J. **139,** 1195.
Lynden-Bell, D. (1965). Astrophys. J. **142,** 1648.
Ostriker, J. P. (1970). *Stellar Rotation,* edited by A. Slettebak (Reidel, Dordrecht), p. 147.
Richtmyer, R. D., and Morton, K. W. (1967). *Difference Methods for Initial Value Problems* (Wiley, New York), 2nd ed.
Roxburgh, I. W. (1966). Astrophys. J. **143,** 111.
Sanders, R. H. (1977). Astrophys. J. To be published.
Sanders, R. H., and Prendergast, K. H. (1974). Astrophys. J. **188,** 489.
Stoeckly, R. (1965). Astrophys. J. **142,** 208.